SCIENTIFIC CULTURE
www.sci-cult.com

SCIENTIFIC CULTURE, Vol. 10, No. 3, (2024), pp. 57-76
Open Access. Online & Print

DOI: 10.5281/zenodo.12738319

ARCHAEOMETRIC STUDY OF PITHOI FROM BULGARIAN ARCHAEOLOGICAL SITES

Bilyana Kostova*[1], Katerina Mihaylova[2], Boyan Dumanov[3] and Ralitza Berberova[1]

[1]New Bulgarian University, Department of Natural Sciences, 21 Montevideo Blvd., 1618 Sofia, Bulgaria
[2]Institute of Mineralogy and Crystallography "Acad. Ivan Kostov", Bulgarian Academy of Sciences, Acad. G. Bonchev Str., bldg.107, 1113 Sofia, Bulgaria
[3]New Bulgarian University, Department of Archaeology, 21 Montevideo Blvd., 1618 Sofia, Bulgaria

Received: 12/07/2024
Accepted: 21/07/2024
Corresponding author: bkostova@nbu.bg

ABSTRACT

An archaeometric study of pithoi from Bulgarian archaeological sites was carried out using analytical techniques such as powder X-ray diffraction (PXRD), Fourier transform infrared (FTIR) spectroscopy, and thermal and X-ray fluorescence (XRF) analysis. New data was obtained – the composition of raw clay (montmorillonite-illite clay with different clay/non-clay minerals ratios) and the firing temperature of the ceramic were determined (three firing temperature ranges: up to 500°C, between 500 and 700°C and between 700°C, and the thermal decomposition temperature of calcite). The advantages of thermal analysis were used to calculate the loss on ignition (LOI) for the correction of the XRF results. The porosity of the ceramic was determined by thermal analysis and FTIR, and a linear functional relationship was established: an increasing density of the structure with an increasing firing temperature. The experimental results show continuity in the raw materials and technologies used to produce ceramic from the Roman Age to Late Antiquity. This supports the archaeological interpretation of a transformation of economic settlement models with a preservation of demographic composition in the region of the Sarnena Sredna Gora and the southern foothills (Bulgaria).

KEYWORDS: pithoi, Bulgarian archaeological sites, analytical techniques, characterization, porosity, firing temperature

1. INTRODUCTION

Pithoi are large ceramic vessels whose use and production have been widespread in the Mediterranean for a long period of time, from the Late Neolithic period to the present. Their size and storage capacity can vary, with a height of 0.50 m to 1.80 m or more, and a capacity between 100 and 800 l, sometimes even reaching up to 1600 l (Ximeri, 2017). Pithoi were mainly used for the storage of liquid and dry foodstuffs like wine, olive oil, grain, and were a preferred food storage container due to their higher technical performance, such as achieving better temperature control and being more vermin-resistant in comparison with many other food storage jars. Additionally, pithoi were used for burial purposes, with the vessels serving as coffins (Bevan, 2018).

Because of their large size and difficulties with transportation, it is generally assumed that pithoi are locally produced – either by travelling specialists or in specialized workshops (Kibaroğlu and Thumm-Doğrayan, 2013; McLoughlin, 2000). The process of pithos manufacturing is a demanding one and as such, pithoi are considered to be a form of specialized pottery production (Porta, 2021). Such large pots call for the application of multiple coils or slabs of clay and sometimes the use of a tournette and/or external bands is needed to reinforce joins. In order to produce such objects in large quantities and of consistent quality, considerable kiln infra-structure is required, as well as exceptional potting skills. Because of this, the potters who made them specialized explicitly in pithoi production. It is suggested that pithos makers were often itinerant – they would travel from place to place, either taking their skills on a tour of already existing customers or looking for new opportunities (Bevan, 2018). In (McLoughlin, 2000), Beatrice McLoughlin notes the phenomenon of pithos makers travelling periodically between several different settlements in Greece, which is evident from the presence of pithoi sherds belonging to more than one style.

The finding of pithoi at a site serves as an indication that the discovered settlement is an organized one. Therefore, the study of such storage vessels is of great importance for the site, as it allows for the further study of its domestic and public economies. There are several approaches to studying pithoi production, one of which is via analytical techniques. Such studies are essential, since the analytical methods applied make it possible to locate the sources of provenance of the ancient samples' raw materials and can thus find their place of manufacture. Furthermore, they can determine the types of clay (calcareous – carbonate-rich or non-calcareous – carbonate-poor) used, the firing temperature of the samples, as well as other characteristics that give additional information regarding the technical know-how of the pithos makers during different periods of time. This research can eventually be compiled together to create a database for comparisons over time (Giannopoulou, 2010).

For the prehistoric period of the Bronze Age, where settlement sites have been of considerable importance, there have been numerous studies that address the socio-economic significance of pithoi, along with ceramic analyses focusing on pottery production technology, with special attention on pithoi (Kibaroğlu and Thumm-Doğrayan, 2013; McLoughlin, 2000; Porta, 2021; Lis and Rückl, 2011; Waiman-Barak et al., 2018; Xanthopoulou et al., 2022). However, for the Classical period and later, where the emphasis has been on sacred sites and cemeteries, the study of pithoi is rather simplistic, providing no more than cursory catalogue descriptions for the most part (McLoughlin, 2000).

The socio-economic importance and lack of adequate research on pithoi production technology after the Bronze Age prompted the selection of pithoi as the objects of the present archaeometric study. The studied ceramic was collected from Bulgarian archaeological sites from the region of Sarnena Sredna Gora and the southern foothills. The samples date from the Roman Age and Late Antiquity. The archaeological investigations in this area have established a change in the location and settlement pattern, from open settlements located at low altitudes during the Roman Age to fortified settlements located in the higher parts of the area during the Late Antiquity. From an archaeological point of view, the change that occurred was driven by financial and economic crises and occurred without demographic changes (Dumanov, 2005; Dumanov, 2017).

The first objective of the archaeometric study of the pithoi is to obtain mineralogical data on their composition and to determine the equivalent firing temperature. The second objective is to obtain information on the raw material used for the production of the pithoi: clay type (calcareous or non-calcareous) and mineral composition of the clay, which will be provided by the mineral composition of the pithoi (Fierascu et al., 2020). The raw material results, in combination with the equivalent firing temperature of the pithoi, will help establish the presence/absence of knowledge continuity about the environment and traditions of the people from the earlier to the later archaeological period in the studied area, which is the third main objective of the work. The archaeometric survey will either support or refute the archaeological perspective on the realized settlement pattern change in the area without the occurrence of a demographic

one. Furthermore, the research will support the transition from archaeological perspectives (conjectures) to empirical knowledge. The results will also complement the sporadic experimental data on pithoi dated after the Bronze Age.

Archaeometric investigations are conducted using a variety of analytical methods, and it is of great importance to use a range of complementary methods to achieve the best results in terms of quality and amount of obtained data (Garrison, 2016). In relation to the objectives of the present study, the following methods were chosen: X-ray diffraction (PXRD), Fourier transform infrared spectroscopy (FTIR), X-ray fluorescence (XRF) and thermal analysis (simultaneous TG/DTG-DSC). The combination of these methods is appropriate and has been used frequently by other authors (Drebushchak et al., 2005; Papadopoulou et al., 2006; Ravisankar et al., 2010; Yan et al., 2021; Palanivel and Kumar, 2011; Cardiano et al., 2004; Nagwa and Rahim, 2016).

PXRD, FTIR, and thermal analysis were used to study the mineral composition of the ceramic, supported by XRF results. PXRD is a method that registers small-sized phases that other methods (e.g., petrographic) cannot register (Xanthopoulou et al., 2020). The method has limitations in registering phases in small quantities (Moropoulou et al., 1995). A disadvantage in the study of ceramic by PXRD is the inability to prepare an oriented sample of clay and meta-clay minerals. When studying raw clay, this approach is used in order to increase the reflection intensity of clay/meta-clay minerals (Xanthopoulou et al., 2020). As such, when examining ceramic, the intensity of the clay/meta-clay minerals is reduced, which can make their registration difficult. In relation to the above-mentioned limitations and disadvantages, PXRD is successfully combined with FTIR. It is a widely used method for the identification of minerals without restrictions on their content percentage in the sample and variations at structural level, thus providing easy identification of clay and meta-clay minerals (Garrison, 2016; Xanthopoulou et al., 2020; Tarhan et al., 2022). Thermal analysis is an important method for confirming the mineral composition of ceramic by tracing processes such as dehydration, dehydroxylation, decarbonation, and mineral structure decomposition (Brown and Gallagher, 2003; Nagwa and Rahim, 2016). The method also registers and assesses the processes of rehydration and rehydroxylation of layered silicates that take place when ceramics are buried over time (Kloužková et al., 2016). The determination of the mineral composition of the ceramic is also supported by XRF data. The measured contents of the major elements Si and Al (represented as ratios of the elements or their oxides) provide information on the type of clay mineral (Shoval and Paz, 2015; Khalifa et al., 2019).

In order to determine the firing temperature of the ceramic (i.e. equivalent firing temperature), the mineral (structural phases formed by a natural process) and phase (structural high-temperature synthetic phases formed in the firing process) composition of the ceramic, determined by PXRD, is often used (El Ouahabi et al., 2015; Aras and Kiliç, 2017). Another approach is using FTIR (Yan et al., 2021). Thermal analysis is also suitable for determining the firing temperature (Waiman-Barak et al., 2018; Kotryová et al., 2016). In the present work, the advantages of all three methods (Palanivel and Kumar, 2011) are used to determine the equivalent firing temperature, with the results supported by loss on ignition (LOI) values (Daghmehchi et al., 2018) determined by thermal analysis. Thermal analysis is a proven correct approach for LOI determination (Frangipane et al., 2008; Shaltout et al., 2012), and its use for such purposes is defined as a fast, energy and sample volume-saving approach, making it preferable to the conventional one (Shaltout et al., 2012). The use of this approach for LOI determination is new for archaeological ceramic samples. The novelty of the work is also the linear relationship between the porosity and the firing temperature of the ceramic, established only by the results from thermal and FTIR analysis.

2. MATERIALS AND METHODS

2.1. Materials, geological and archaeological background

Eleven pithoi sherds (Fig. 1) from 11 Bulgarian archaeological sites in the area of the Sarnena Sredna Gora and the southern foothills (Fig. 2) were studied.

The studied samples, their respective archaeological sites and archaeological periods are presented in Table 1.

Figure 1. Representative samples of analyzed pithoi sherds – No. 10 (arhaeological site No. 17 Gorno Novo Selo village, fortified settlement, Late Antiquity), No. 86 (arhaeological site No. 6 Malko Tranovo village, open settlement (vicus), Roman Age) and No. 115 (arhaeological site No. 21 Sarnevets village, Late Antiquity).

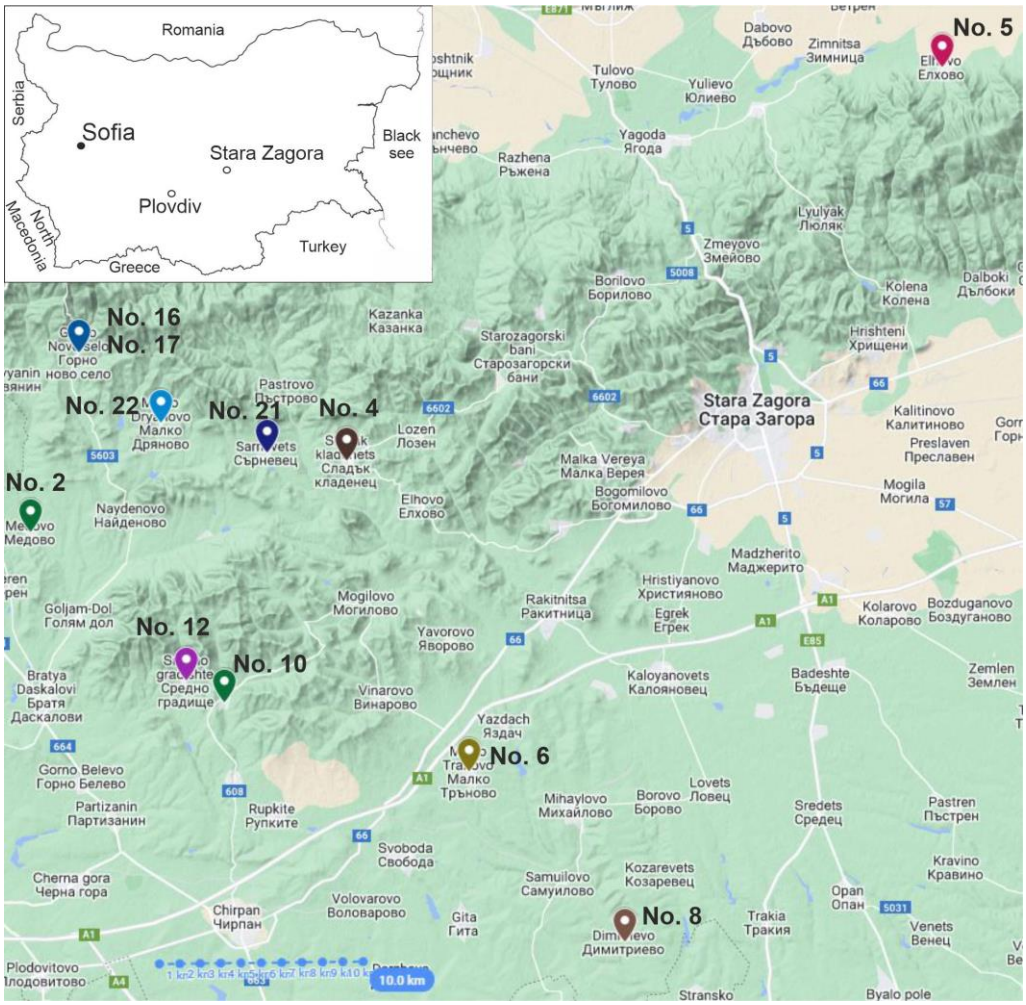

Figure 2. Geographical position of the archaeological sites (the numbers correspond to the catalogue number of the archaeological sites listed in Table 1).

Table 1. Samples, archaeological sites, and archaeological periods.

Sample	Archaeological site	
	Catalogue No, location, type	Period
No. 38	No. 2 Medovo village, open settlement	Roman Age
No. 51	No. 8 Dimitrievo village, open settlement (*Emporion Pizos*)	
No. 86	No. 6 Malko Tranovo village, open settlement (*vicus*)	
No. 92	No. 5 Elhovo village, Roman villa "Chatalka"	
No. 125	No. 4 Sladak kladenets village, open settlement	
No. 10	No. 17 Gorno Novo Selo village, fortified settlement	Late Antiquity
No. 19	No. 16 Gorno Novo Selo village, church *Extra Muros 2*	
No. 29	No. 12 Sredno gradishte village, fortified settlement	
No. 69	No. 10 Izvorovo village, Golyamoto gradishte area, fortified settlement	
No. 115	No. 21 Sarnevets village	
No. 132	No. 22 Malko Dryanovo village	

The following rocks are revealed on the ground surface at the archaeological sites: pre-Cambrian (Archaic) metamorphic gneisses composed of quartz, muscovite, albite, and microcline (sites No. 5, 16, 17, and 22); Paleozoic granitoids composed of plagioclase, microcline, quartz, biotite, muscovite, and weathering minerals – sericite, chlorite, and clays (site No. 2); Mesozoic upper Cretaceous sedimentary – limestones, sandstones, and marls (sites No. 4, 10, and 12) and volcanogenic sedimentary rocks – alternation of tuffs, sandstones, marls, limestones (site No. 21); Oligocene limestones (site No. 6); Neogene sedimentary rocks – gravels, sands, and clays (site No. 8) (Boyanov et al., 1991; Boyanov et al., 1993; Tsankov et al., 1995). No clay deposits were found during the fieldwork from which samples could be taken for comparison with the ceramic in order to identify them as a likely source material. Modern geological knowledge of the area is used to search for deposits in the vicinity of the archaeological sites, but it should be noted that current deposits may not have been exposed on the ground surface in the past and may not have been known. In addition, deposits that existed in the past may have been depleted or hidden to the present day due to changes in the landscape, urbanization, etc. (Xanthopoulou et al., 2020). It has been found that clay deposits can be located at varying distances from the site of ancient pottery production, from less than 1 km to 50 km, with the final cost of pottery increasing with distance (Xanthopoulou et al., 2020).

During the Roman imperial period (1st–4th centuries AD), two settlement patterns were widespread: villa farms and open villages (vicus; pl. vici) located in areas with slightly hilly topography and relatively low altitude (200-300 m). The Roman villa complex "Chatalka" in the village of Elhovo (site No. 5), includes two distinct architectural units - residential and rural. Other structures have been found around them - a pagan shrine, an early Christian church, a bathhouse, kilns for producing ceramic building and household materials. The residential unit (pars urbana) has a total area of 1300 m^2 and includes representative housing and housing for the service staff. The rural unit (pars rustica), from which the samples were taken, has an area of 6500 m^2 and two distinct sections. One is related to the production of building and household ceramics, the other is domestic and includes stables, a granary (horreum), storerooms and houses for the workers and the manager (Nikolov, 1984). The main form of settlement in the Roman Age were the vici – agricultural unfortified settlements, which consisted of widely dispersed households located in parts of arable land. Such are sites No. 2, 4, 6, and 8 (Boyanov, 2014) (Table 1). For site No. 6, the materials diagnostic of the site's age are late Roman fibulae and coins, the latest of which are of Emperor Valens (364-378). This indicates an upper age limit in the existence of the vicus - the late 4th or early 5th century, when it was abandoned as a consequence of the Gothic migration processes (Dumanov, 2005; Wendel, 2020). The villas and vici were the basis for economic stability and the development of the Roman agricultural economy, with a primary focus on crop production.

At the end of the 4th century, the local economic situation changed in relation to the period of human migration and barbarian invasions (the Migration Age). The large Roman villas and vici disappeared in the middle of the 5th century after the reforms and reconstructions of the emperors Anastasius I (495–518) and Justinian I (527-565). As a result, a new type of settlement model emerged during the Late Antiquity, located away from the old Roman settlements - fortified highland settlements (Dumanov, 2017) (sites No. 10, 12, 16, 17, and 21 (Table 1). After these changes, agriculture remained limited in the territories and surroundings of the fortified settlements, as the former arable land was left to the new population of migrants who preferred a nomadic or semi-nomadic economy. In order to provide security for the population, the new structures (fortified settlements) were located at a higher altitude, probably combining rural and military functions. Due to the mountainous landscape, the agricultural potential of the fortified settlements was limited, and the inhabitants were taught animal husbandry. Thus, the fortified settlements became dependent on grain shipments, but their inhabitants were able to exploit all local sources of raw materials. Fortified settlements emerged en masse in relation to the need to transform economic models in an era of financial and economic crises and due to the seizure of former settlement territories by new migrant populations. The archaeological studies clearly show precision in the choice of the location for the construction of the new sites, the planning of the fortification and the location of the most important internal buildings, especially the churches, but also the warehouses and water supply facilities (Dumanov, 2017; Kostova et al., 2023a).

2.2. *Methods*

Sample preparation: before grinding, the samples were mechanically cleaned using a brush and purified with distilled water. A very thin section of the outermost layer of the pithoi was removed (i.e., the parts that were in direct contact with the environment) in order to analyze solely the non-altered material (Cardiano et al., 2004). The samples were then ground to powder using an agate mortar.

Powder X-ray diffraction (PXRD) measurements were made by D2 Phaser Bruker AXS, CuKα radiation

(λ = 0.15418 nm) (operating at 30 kV, 10 mA) from 3 to 70°2θ with a step of 0.05°, 1 s/step (ground sample weight – 1.0±0.1 mg and particle size below 0.075 mm). The PDF database was used for determining the phases and minerals in the samples (File, 2001). The database was indexed in the computer program for qualitative analysis QualX (v. 2.24), where phase identification and peak fitting were performed (Altomare et al., 2008). The analysis was used to determine the inorganic phases in the samples.

Fourier transform infrared (FTIR) measurements were performed by FTIR Spectrometer Nicolet 6700, covering the range of 400 - 4000 cm^{-1} with 100 scans and 1.928 cm^{-1} resolution. The samples were prepared as pellets with KBr. The analysis was used to determine the inorganic and organic phases in the samples.

Thermal analysis: simultaneous TG/DTG-DSC analysis was carried out on a Setline STA 1100, SETARAM, France, in the temperature range room temperature (RT) – 900°C; in static air, with a heating rate of 10°C min^{-1}. The operational characteristics of the TG/DTG–DSC – system are: sample mass of 25.0±1.0 mg (mass resolution of 0.05 μg), temperature resolution of +/- 0.3°C, and alumina sample crucible with a volume of 100 μL. Thermal analysis was used to determine the behavior of the samples upon heating – mass loss and dehydration temperature, dehydroxylation and destruction of organic and inorganic phases. The samples were not heated above 900°C as it was determined that the latter effects occurring with mass loss take place at a maximum temperature of 886.6°C (Table 2). Above this temperature, crystallization of high-temperature oxygen-bearing phases begins – ones with spinel-type structure, mullite, cordierite, cristobalite (Brown and Gallagher, 2003; Shoval and Paz, 2015; El Ouahabi et al., 2015), which is associated with oxygen uptake from the atmosphere and an increase in sample weight. The method was implemented for the determination of LOI in XRF, to determine the equivalent firing temperature of the ceramic, and to analyze its porosity.

X-ray fluorescence (XRF) analysis was used for the determination of the chemical composition of the samples. The measurements were performed by spectrometer WD-XRF Supermini 200 - Rigaku, Japan (50 kV and 4mA, 200 W X-ray tube with Pd-anode, 30 mm^2) in a helium atmosphere. Two different X-ray detectors, a gas flow proportional counter for light elements and a scintillation counter for heavy elements are used. Depending on the wavelength range, three analyzing crystals were used: LIF 200 (for Ti-U), PET (for Al-Ti) and RX25 (for F-Mg). Before measurement, the samples were ground to powder, then dried at 100°C until reaching constant weight (Frangipane et al., 2008; Shaltout et al., 2012; Kenkel, 2014; Ramos et al., 2002). Rigaku's built-in software package ZSX was used for the processing of the data. LOI was determined by thermal analysis for each sample and accounted as an input parameter by the built-in software package (Shaltout et al., 2012). LOI was calculated for each sample by summing up the mass loss (ML) in the temperature ranges in which volatile components are released (Kenkel, 2014; King and Vivit, 1988) and alkali cations evaporate (Derkowski and Kuligiewicz, 2022).

3. RESULTS

3.1. PXRD results

The PXRD results are presented in Fig. 3. Through PXRD, the following phases were found in all samples: illite (general formula $(Si_{4-x}Al_x)^4(Al_{2-y}Mg_y)^4O_{10}(OH)_2(x+y)K^+$ (Bergaya et al., 2006) (PDF#02-0056), muscovite (general formula $(Si_3Al)^4(Al_2)^6O_{10}(OH)_2K^+$ (Bergaya et al., 2006) – PDF#34-0175), montmorillonite $(M^+_y \times nH_2O)(Al_{2-y}Mg_y)Si_4O_{10}(OH)_2$, where M = Na^+, K^+, Ca^{2+}, Mg^{2+}, Fe^{3+} (Bergaya et al., 2006) – PDF#07-0304, quartz (SiO_2 – PDF#06-175), and plagioclase – albite ($NaAlSi_3O_8$ – PDF#89-6426).

Since muscovite and illite are isostructural, their PXRD peaks coincide (Fig. 3) and as such it is difficult to distinguish them by this method (Kotryová et al., 2016; Chamley, 1989). The registration of montmorillonite in ceramic is possible because it retains its structure after (i) dehydration, which takes place at temperatures in the range 100-180°C (Garg and Skibsted, 2015; Liu et al., 2011) until 200°C (Garg and Skibsted, 2015); (ii) partial dehydroxylation at around 460°C and (iii) dehydroxylation, which takes place in the temperature range 600-700/800°C (Garg and Skibsted, 2015; Grim and Kulbicki, 1961; Hatakeyama and Liu, 1998; Labus et al., 2023).

The breakdown of the montmorillonite structure is marked by the disappearance of diffraction effects and begins after 800°C (Garg and Skibsted, 2015; Labus et al., 2023; Khalifa et al., 2019), and according to Grim (Grim and Kulbicki, 1961) – after 850-900°C for Cheto-type montmorillonite and after 900-950°C for Wyoming-type montmorillonite. For thermally treated montmorillonite (heated or meta-montmorillonite, also referred to as meta-smectite), the diffractograms show: (i) a decrease in d_{001} from 15Å (PDF#13-0135) – 14.5Å (Khalifa et al., 2019) to 9.80Å (measured during heating of montmorillonite to 200°C (Khalifa et al., 2019) and to 9.70Å (measured during heating of montmorillonite to 725°C (Bradley and Grim, 1951); (ii) an increase in reflex intensity (003) (Grim and Kulbicki, 1961) and (iii) the reflex intensity (002) remains without significant changes

(Grim and Kulbicki, 1961). The shifted position of the basal reflex (001) of heated montmorillonite coincides with the reflex (002) of illite and muscovite (Khalifa et al., 2019) (Fig. 3)

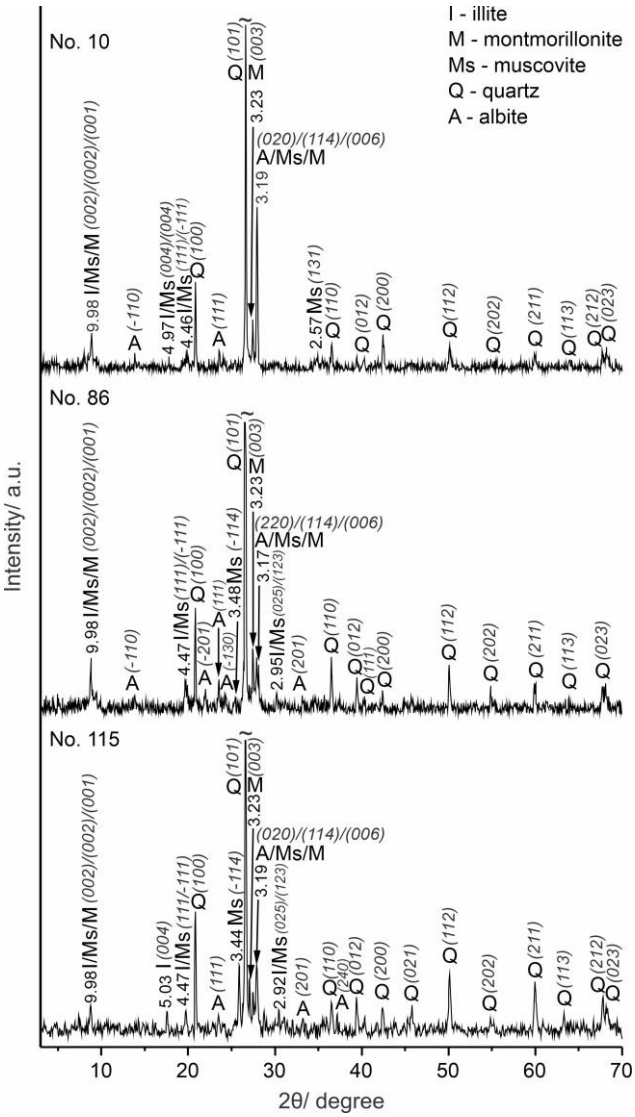

Figure 3. Representative PXRD patterns and (hkl) planes (Miller indices) of samples No. 10, No. 86, and No. 115, with additional d-values for the layered silicates.

3.2. FTIR results

Figure 4 presents the results from the FTIR analysis. The results confirm those of the PXRD analysis, while additionally proving the presence of calcite ($CaCO_3$), hematite (Fe_2O_3), microcline ($K(AlSi_3O_8)$), and organic phases in all samples.

In the spectral range 3800 – 3700 cm^{-1}, an O-H band was registered (3734-3736 cm^{-1}), assigned to the surface hydroxyl group absorbed from the air (Chukanov and Chervonnyi, 2016).

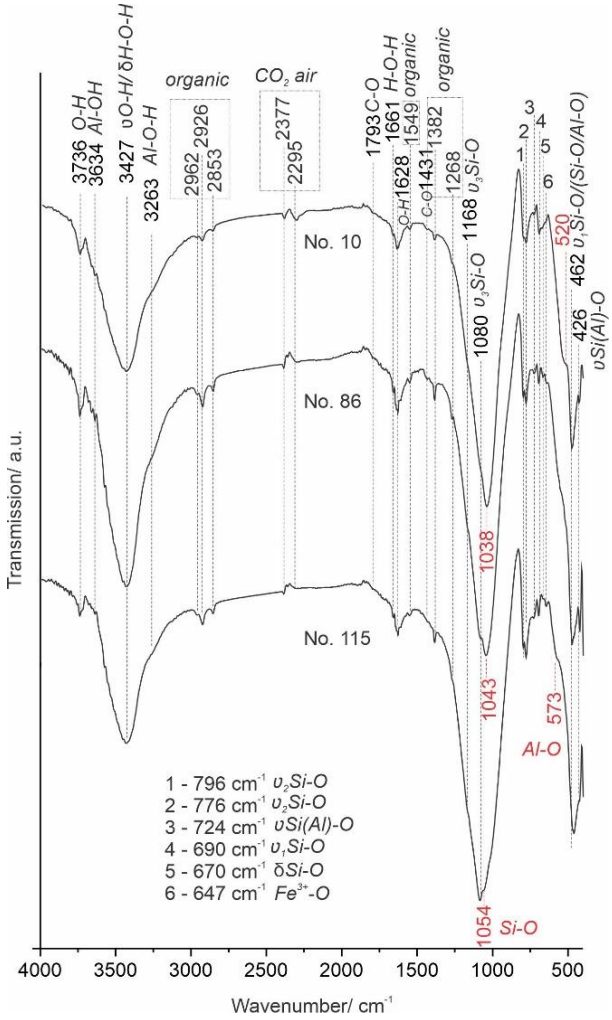

Figure 4. Representative FTIR spectra of samples No. 10, No. 86, and No. 115 (4000 - 400 cm^{-1} spectral region).

O-H and M-O (M – metal) vibrational bands assigned to mica and clay (muscovite, illite and montmorillonite) are registered in the ranges 3700-3500 cm^{-1} and 1700-1550 cm^{-1} (Daghmehchi et al., 2018). The band at 3634-3637 cm^{-1} is associated with Al-OH stretching vibration of illite and montmorillonite (Chukanov, 2014; Caccamo et al., 2020). The broad band with center at 3427-3432 cm^{-1} corresponds to the vO-H stretching vibration of H_2O in montmorillonite (Caccamo et al., 2020) heated below the amorphization temperature. This band is also associated with a bending δH-O-H vibration of H_2O in an amorphous clay phase (when the ceramic is fired and reaches a temperature leading to the decomposition of the clay structure (Daghmehchi et al., 2018) but the observed PXRD peaks of montmorillonite reject this assignment. The shoulder at 3262-3263 cm^{-1} is associated with Al-O-H stretching vibration of montmorillonite) (Chukanov, 2014; Caccamo et al., 2020). The band at 1658-1661 cm^{-1} was recognized as the H-O-H bending vibration of adsorbed water molecules of illite, and the one at 1628-1631 cm^{-1} as the O-H stretching vibra-

tion of adsorbed water molecules of illite and muscovite (Daghmehchi et al., 2018; Chukanov, 2014; Caccamo et al., 2020). Registration of hydroxyl bonds in layered silicates type 2:1 (illite, muscovite, montmorillonite) is possible because dehydration and rehydration processes are reversible with time in isothermal low-temperature conditions (Kotryová et al., 2016; Derkowski and Kuligiewicz, 2022; Hamilton and Hall, 2012; Muller et al., 2000), provided that they are not heated at temperatures exceeding the decomposition and amorphization temperatures of their structure (Daghmehchi et al., 2018).

In the spectral ranges 2900-2700 cm^{-1} and 1900-1200 cm^{-1} vibrations assigned to organic phases were recorded: C-H asymmetrical stretching vibrations of CH_2 at 2962-2963 cm^{-1}, 2923-2926 cm^{-1} and 2853-2854 cm^{-1}, along with the bands at 1549 cm^{-1} (C-O skeletal vibrations of the aromatic ring), 1382 cm^{-1} (C-H bending vibrations of the methyl and methylene groups) and 1267-1268 cm^{-1} (ν_3 stretching vibration of C-O in aromatic rings) (Yan et al., 2021; Chukanov, 2014; Rao et al., 2017).

Bands, centered at 2377-2385 cm^{-1} and 2295-2297 cm^{-1} in the range 2400-2300 cm^{-1} are assigned to CO_2 from the air (Chukanov and Chervonnyi, 2016).

The bands at 1793-1796 cm^{-1} and 1431-1432 cm^{-1} are identified as ($\nu_1+\nu_4$) C-O in CO_2^{-3} and (ν_3C-O in CO_2^{-3}) in calcite (Chukanov, 2014).

Metal-oxygen vibrations, mainly Si-O and Al-O vibrations of silicates and aluminosilicates are registered in the spectral range 1300-400 cm^{-1} (Tarhan et al., 2022). The shoulders at 1168-1170 cm^{-1} and 1079-1080 cm^{-1} (ν_3Si-O asymmetrical stretching vibration) are characteristic of quartz; in addition to the bands at 796 cm^{-1}, 776-777 cm^{-1} (ν_2Si-O symmetrical stretching vibration), 690-691 cm^{-1} (ν_1Si-O in SiO2), and the band close to 460 cm^{-1} (Shoval and Paz, 2015; Daghmehchi et al., 2018; Chukanov, 2014). The band at 460 cm^{-1} is a combination of Si-O bending vibration of quartz and Si-O/Al-O bending vibration of a heated clay phase (Daghmehchi et al., 2018; Annamalai et al., 2014). The band at 1031-1055 cm^{-1} is attributed to Si-O stretching vibration of illite and heated montmorillonite (Palanivel and Kumar, 2011; Tarhan et al., 2022; Shoval and Paz, 2015; Daghmehchi et al., 2018). The bands at 520 cm^{-1} and 570 cm^{-1} are recognized as (Al-O) vibrations of illite and montmorillonite (Yan et al., 2021; Chukanov, 2014; Caccamo et al., 2020). The band at 724 cm^{-1} is assigned to vSi (Al)-O stretching vibration of albite, and the one at 426 cm^{-1} – to microcline (Chukanov, 2014; Annamalai et al., 2014). The band at 647 cm^{-1} is located in the same range, and is identified as Fe^{3+}-O vibration of hematite (Chukanov, 2014; Jozanikohan and Abarghooei, 2022).

3.3. Thermal analysis results

Table 2 and Fig. 5 show the thermal analysis results. The registered mass loss (ML) was divided into five temperature ranges: RT-220°C (dehydration), 220-420°C (organic decomposition), 420-770°C (dehydroxylation), 770-840°C (decarbonation) and 840-900°C (structure destruction). The total mass loss (ML_{tot}) changes from 4.02% (No. 115) to 13.57% (No. 29).

Table 2. Thermal analysis results.

Sample	RT-220°C dexydration				220°C-420°C organic decomposition		420°C-770°C dehydroxylation		770°C-840°C decarbonation		840°C-900°C structure destruction		ML_{tot}/ %
	T_{infl}/ °C	ML/ %	T_{infl}/ °C	ML/ %	T_{infl}/ °C	ML/ %	T_{infl}/ °C	ML/ %	T_{infl}/ °C	ML/ %	T_{infl}/ °C	ML/ %	
Roman Age													
No. 38	27.5	0.20	123.0	0.36	253.2	0.76	460.9	0.52	810.5	0.13	843.1	0.13	5.85
	84.9	0.42	165.9	0.15	341.1	0.61	569.3	0.27			865.6	0.46	
			218.8	0.70	385.5	0.37	640.7	0.27					
							692.5	0.40					
							753.6	0.12					
No. 51	38.6	0.51	113.6	0.22	266.8	0.20	461.2	0.44	802.8	0.27	849.3	0.20	4.45
	61.1	0.59	147.0	0.34	305.7	0.29	573.4	0.13					
			196.8	0.31	383.9	0.30	677.5	0.43					
							760.8	0.08					
No. 86	52.4	0.29	117.7	0.40	266.3	0.29	453.7	0.29	785.5	0.08	886.6	0.10	4.50
	80.9	0.78	134.6	0.18	283.7	0.10	530.6	0.13					
			149.3	0.21	324.2	0.34	636.0	0.07					
			179.3	0.19	391.6	0.36	662.3	0.10					
							700.3	0.18					
No. 92	50.4	0.59	102.4	0.59	367.3	0.91	467.8	0.82	810.9	0.28	838.0	0.26	11.93
	80.3	1.19	125.3	0.64	334.9	0.96	573.4	0.91			872.4	0.46	
			146.8	0.36	392.3	0.54	699.9	1.34					
			168.2	0.27			762.2	0.16					

			203.1	0.92									
No. 125	38.8	0.46	121.2	0.29	262.3	0.58	440.2	2.00	814.8	0.32	844.8	0.28	11.28
	78.9	0.76	130.9	0.30	335.1	1.17	559.2	0.95			880.2	0.39	
	97.2	0.47	205.4	1.27			672.1	1.46					
							762.2	0.28					
Late Antiquity													
No. 10	54.1	0.48	106.5	0.60	238.2	0.44	468.0	2.03	808.8	0.41	866.6	0.55	12.30
	80.9	1.26	125.7	0.85	265.2	0.53	562.7	0.70					
			163.1	0.38	321.5	0.52	632.0	0.37					
			192.8	0.53	348.5	0.48	674.1	0.46					
					388.0	0.35	708.8	0.48					
							764.1	0.41					
No. 19	50.6	0.56	124.5	0.60	252.3	0.44	466.2	1.14	809.3	0.28	843.1	0.24	11.24
	76.2	1.55	147.6	0.35	325.9	0.80	515.1	0.52			874.7	0.22	
			132.0	0.39			572.9	0.36					
			214.6	0.50			680.0	1.18					
							748.8	0.27					
No. 29	52.7	0.41	107.3	0.83	247.8	0.44	448.2	1.76	812.0	0.25	841.0	0.33	13.57
	84.4	1.61	122.8	0.80	326.0	1.09	531.3	0.60			882.3	0.35	
			173.8	0.44	372.1	0.69	577.2	0.59					
			199.0	0.57			644.4	0.69					
							716.2	0.83					
No. 69	48.7	0.74	105.1	0.52	257.8	0.77	475.9	1.24	817.5	0.34	834.6	0.21	12.94
	80.3	0.94	118.5	0.60	335.1	0.60	496.3	0.74			865.2	0.45	
			190.3	1.16	375.8	0.56	576.3	0.44					
							621.9	0.37					
							687.7	1.36					
							759.5	0.30					
No. 115	65.7	0.26	36.4	0.26	230.1	0.34	450.9	0.26	811.0	0.14	848.5	0.10	4.02
			163.7	0.18	273.0	0.37	499.2	0.19			878.6	0.15	
					321.9	0.32	570.5	0.26					
					369.0	0.26	643.8	0.25					
					405.9	0.25	695.2	0.30					
							763.7	0.13					
No. 132	45.9	0.30	104.7	0.41	258.0	0.60	446,7	0.76	813.2	0.18	856.7	0.29	8.18
	77.6	0.87	126.7	0.99	318.0	0.63	507,2	0.23					
			187.8	0.18	385.5	0.55	537,9	0.20					
			203.3	0.28			575,3	0.16					
							706,1	0.62					
							769,4	0.17					

T_{infl} – temperature of the point of inflection/°C
ML – mass loss/%;
ML_{tot} – mass loss total/%

Two thermal events occur during the first temperature range: dehydration – up to 100°C, the physically adsorbed water molecules evaporate (Ion et al., 2010) and between 100°C and 220°C, the phyllosilicates (i.e. sheet silicates: montmorillonite, illite, and muscovite) dehydrate (Brown and Gallagher, 2003; Grim and Kulbicki, 1961). The mass loss between RT and 100°C ($ML_{RT-100°C}$) changes from 0.26% (No. 115) to 2.33% (No. 19), and the one between 100 and 220°C ($ML_{100-220°C}$) from 0.44% (No. 115) to 2.78 (No. 92) (Table 2).

During the second temperature range (220-420°C), the exothermal effect of organic decomposition is registered at around 330°C (Palanivel and Kumar, 2011). The process occurs with ML ($ML_{220-420°C}$) from 0.79% (No. 51) to 2.41% (No. 92) (Table 2). The registration of more than one peak on the DTG curve in this temperature range is associated with a step-wise progression of pyrolysis (Labus et al., 2023).

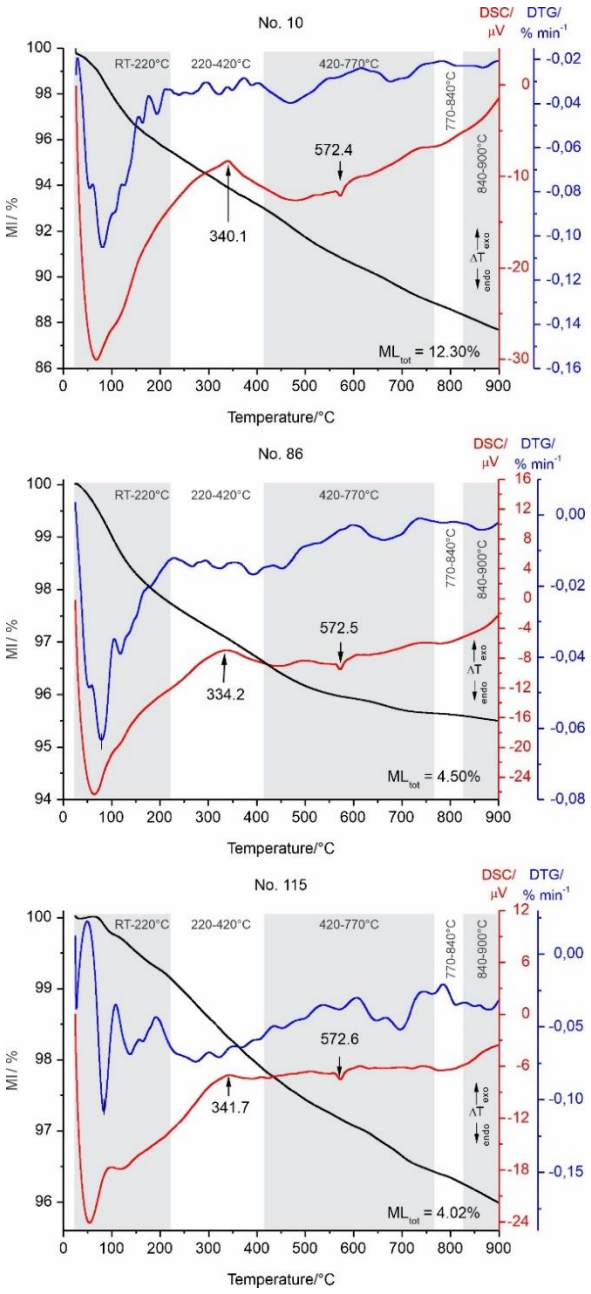

Figure 5. Thermal analysis results – TG, DTG, and DSC curves of representative samples No. 10, No. 86 and No. 115.

Two thermal processes occur during the dehydroxylation temperature range (420–770°C). The first process is recognized as α-β polymorphic transition of quartz, occurring with an endothermal peak on the DSC curve near 572°C (Fig. 5) and without ML (Moropoulou et al., 1995). The second process is dehydroxylation of phyllosilicates and occurs with ML ($ML_{420\text{-}770°C}$) from 0.77% (No. 86) to 4.69% (No. 125) (Table 2). At a temperature of about 460°C, montmorillonite releases the tightly bound water from the interlayer space, which is accompanied by partial dehydroxylation (Liu et al., 2011). The effect is registered at temperatures (T_{infl}) from 440.2°C (No. 125) to 475.9°C (No. 69) (Table 2). Dehydroxylation of illite occurs at temperatures between 520-590°C (Marsh et al., 2018). In the studied samples, it was registered at T_{infl} from 507.2°C (No. 132) to 576.3°C (No. 69). Dehydroxylation of muscovite occurs in the temperature range 670-690°C (Hatakeyama and Liu, 1998; Földvári, 2011; Pei et al., 2018). The effect is registered at T_{inf} from 672.1°C (No. 125) to 695.2°C (No. 115) in the pithoi samples (Table 2). Complete dehydroxylation of montmorillonite takes place at 690-750°C (Brown and Gallagher, 2003; Garg and Skibsted, 2015; Grim and Kulbicki, 1961), with the process being registered in all samples at T_{infl} from 700.3°C (No. 86) to 769.4°C (No. 132) (Table 2).

Calcite decarbonation was recognized at the temperature range 770-840°C (Böke et al., 2006). The process occurs in all samples, with $ML_{770\text{-}840°C}$ between 0.08% (No. 86) and 0.41% (No. 10) at T_{infl} from 785.5°C (No. 86) to 817.5°C (No. 69) (Table 2).

During the last temperature range 840°C-900°C, an endothermic effect occurs where the structure of dehydroxylated phyllosilicates undergoes decomposition (Fig. 5) (Grim and Kulbicki, 1961; Lee et al., 2008, Pérez-Monserrat et al., 2021). In general, these processes occur without mass loss as the volatile components are already separated from the sample, but at high temperatures (above 800°C), small mass losses can be recorded due to the evaporation of alkali cations (Derkowski and Kuligiewicz, 2022). $ML_{840\text{-}900°C}$ ranging from 0.10% (No. 86) to 0.68% (No. 29) are registered in the studied samples (Table 2).

3.4. XRF results

The XRF analysis results are normalized – a total concentration of 100%, presented as oxides, with the exception of Cl. The LOI values were calculated as the total sum of $ML_{100\text{-}220°C}$ + $ML_{220\text{-}420°C}$ + $ML_{420\text{-}770°C}$ + $ML_{770\text{-}840°C}$ + $ML_{840\text{-}900°C}$ ($ML_{RT\text{-}100°C}$ was not taken into account due to the pre-drying of the samples) (Table 2). The determined LOI values are presented in Table 3 and range from 3.02% (No. 86) to 10.26% (No. 29). The XRF results (Table 3) show that the amount of SiO_2 is the highest in the samples, and it varies from 53.12% (No. 69) to 60.52% (No. 86), followed by Al_2O_3 – between 19.20% (No. 86) and 21.66% (No. 132). The amount of Fe_2O_3 is from 4.91% to 6.53%, and K_2O – from 3.44% to 5.15%. MgO and CaO have low contents between 1.2 and 2.5%. P_2O_5 varies from 1.15 to 1.46% - its presence is related to the registered organic phases in the samples. The oxides of Cr, Zn, Rb, Sr, Cu, and Ag are in negligible quantities: 0.01 – 0.03%.

Table 3. XRF results (mass %).

Oxide	Sample										
	No.38	No.51	No.86	No.92	No.125	No.10	No.19	No.29	No.69	No.115	No.132
SiO_2	59.03	60.01	60.52	56.20	53.88	55.74	56.65	54.11	53.12	58.42	54.28
Al_2O_3	20.47	19.45	19.20	19.31	19.59	19.78	20.67	20.64	19.87	20.79	21.66
Na_2O	-	-	2.09	-	-	-	-	-	-	-	1.48
K_2O	4.93	3.44	3.88	4.48	4.66	4.59	4.28	5.15	4.84	3.89	5.08
MgO	1.48	2.40	1.43	1.43	1.59	1.22	1.52	0.90	1.64	1.78	1.60
CaO	1.85	2.84	2.60	2.40	2.78	1.59	2.10	1.84	2.52	2.43	1.97
TiO_2	0.63	0.69	0.72	0.69	0.75	0.55	0.59	0.62	0.73	0.73	0.74
MnO	0.05	0.15	0.19	0.06	0.09	0.05	0.04	0.06	0.06	0.14	0.05
Fe_2O_3	4.91	6.48	5.08	5.06	5.84	4.92	5.61	5.09	6.22	6.53	5.57
P_2O_5	1.29	1.24	1.15	1.28	1.33	1.33	1.15	1.24	1.22	1.46	1.25
Cr_2O_3	-	-	-	-	-	0.02	0.02	-	-	-	-
CuO	0.02	0.02	0.02	0.01	0.02	0.01	0.01	0.01	0.01	0.01	0.01
ZnO	0.03	0.02	0.02	0.02	0.02	0.02	0.01	0.02	0.02	0.01	0.02
Rb_2O	0.02	0.01	0.02	0.02	0.01	0.01	0.01	0.02	0.01	0.01	0.01
SrO	0.01	0.02	0.03	0.04	0.02	0.01	0.01	0.02	0.03	0.02	0.01
ZrO_2	0.02	0.02	0.03	0.04	0.02	0.01	0.02	0.03	0.02	0.02	0.03
Ag_2O	-	-	-	-	-	0.03	-	-	-	-	-
SO_3	0.03	-	-	0.04	0.10	0.03	0.02	-	0.03	-	-
Cl	0.01	-	-	-	-	-	-	-	-	-	-
LOI	5.25	3.21	3.02	8.92	9.29	10.09	7.29	10.26	9.66	3.76	6.25
Si/Al	2.55	2.72	2.78	2.57	2.43	2.49	2.42	2.32	2.36	2.48	2.21
Al_2O_3/SiO_2	0.35	0.32	0.32	0.34	0.36	0.35	0.36	0.38	0.37	0.36	0.40

4. DISCUSSION

4.1. Mineral composition of pithoi

Inorganic (non-clay and clay minerals - quartz, feldspars, hematite, calcite, illite, montmorillonite, muscovite) and organic phases were found in the studied ceramic fragments.

Quartz is proven by phase methods (Figs. 3, 4) and thermal analysis (Figs. 5). Feldspars: albite is evidenced by PXRD and FTIR (Figs. 3, 4), and microcline – only through FTIR (Fig. 4). The absence of microcline in the diffractograms is related to its small amount in the samples and the low detection limit of PXRD – less than 5% (Moropoulou et al., 1995). Calcite is found only through FTIR and thermal analysis (Figs. 4, 5). From the measured mass loss of CO_2 from calcite decomposition (Table 2), the calcite content in the samples was determined – from 0.18% (No. 86) to 0.92% (No. 10), which explains the absence of this phase in the diffractograms (Moropoulou et al., 1995). Hematite is registered only by FTIR (Fig. 4). PXRD cannot register hematite due to the measurement conditions (CuKα radiation). Measured Fe_2O_3 contents ranged from 4.91% (No. 38) to 6.53% (No. 115) (Table 3) and indicate that iron is present in sufficient quantity to form both its own phases and to incorporate into other minerals – illite (Meunier and El Albani, 2007), montmorillonite (Shoval and Paz, 2015; Bergaya et al., 2006) and plagioclases (Sugawara, 2000). Hematite may be a mineral from the source clay, or it may be a phase formed during the firing of the ceramic by (i) dehydroxylation of goethite under oxidizing conditions at about 300-310°C (Liu et al., 2013; Ponomar, 2018); (ii) oxidation of magnetite at around 500°C (Földvári, 2011); (iii) disintegration of the structure of clay minerals at around 850°C-950°C (Cardiano et al., 2004, El Ouahabi et al., 2015).

Illite, muscovite, and montmorillonite are proven by phase methods (Figs. 3, 4) and thermal analysis (Fig. 5). Their presence is also supported by the chemical analysis results (Table 3). The measured high K_2O contents (from 3.44% for No. 51 to 5.15% for No. 29) support not only the presence of a small amount of

potassium feldspar (microcline), but also of illite (Shoval and Paz, 2015; Khalifa et al., 2019). The presence of illite and montmorillonite is additionally confirmed by the measured MgO content (from 1.22% for No. 10 to 2.40% for No. 51) (Table 3). The inclusion of Mg in montmorillonite is confirmed by the determined decomposition temperature of the montmorillonite structure, between 840 and 880°C, which is characteristic of Cheto-type montmorillonite in which Al is isomorphically replaced by Mg (Grim and Kulbicki, 1961; Földvári, 2011). The presence of montmorillonite is also confirmed by the CaO content in the samples – from 1.59% to 2.84% (Table 3). Thermal analysis results established that only a minimal amount of CaO is included in calcite (Table 2): from 0.10% (No. 86) to 0.52% CaO (No. 10), thus confirming the inclusion of a predominant amount of calcium in the non-calcite phase.

The predominance of Al_2O_3 and SiO_2 indicates that the major composition of the ceramic is of silicate and aluminosilicate origin. The Al_2O_3/SiO_2 ratio (Shoval and Paz, 2015) (or that of Si/Al (Khalifa et al., 2019)) can be used to confirm the type of source clay from which the ceramic was prepared, while recognizing that these ratios may be inflated by an increased quartz content in the ceramic (Shoval and Paz, 2015; Khalifa et al., 2019). The theoretical Si/Al ratio in kaolinite is approximately 1. The determined Si/Al ratio in the studied samples is greater than 1 (Table 3), which is considered an indication that the layered silicates present in the ceramic are type 2:1 (illite, montmorillonite, and muscovite) and/or that the ceramic has a high quartz content (Khalifa et al., 2019). According to Shoval and Paz (2015), an Al_2O_3/SiO_2 ratio of 0.43 to 0.63 is typical for a source kaolinite clay, and an Al_2O_3/SiO_2 ratio in the range of 0.22 to 0.36 is typical for a source montmorillonite clay. In the studied samples, this ratio ranges from 0.32 to 0.40 and, as such, does not reach the minimum value of 0.43 that is determined for kaolinite (Table 3). These results confirm the PXRD and FTIR results for the presence of montmorillonite in the studied ceramic, while the values above 0.36 are very likely related to an increased quartz content in the samples. Further confirmation of a predominant montmorillonite content in the source clay is the dominant FTIR band of heated montmorillonite in the range 1038-1054 cm^{-1} (Shoval and Paz, 2015) (Fig. 4).

4.2. Equivalent firing temperature of pithoi

The inorganic phases present in the ceramic can be used to determine the equivalent firing temperature of the studied samples. Plagioclases are stable up to about 1100/1200°C and are not used in determining the firing temperature along with quartz (Aras and Kiliç, 2017), which is stable until about 840°C when it transitions to tridymite, but peaks of quartz in diffractograms can be recorded up to 1100°C (Bitay et al., 2020). The FTIR-registered hydroxyl bonds in the layered silicates indicate a process of rehydration and/or rehydroxylation, indicating that the firing temperature of the ceramic has not reached the decomposition temperature of their structure (i.e., the stage of amorphization and subsequent crystallization of high-temperature phases has not been reached) (Derkowski and Kuligiewicz, 2022). This is confirmed by the structure decomposition effects recorded by thermal analysis (Fig. 5, Table 2), which start at temperatures above 840°C. The registration of montmorillonite peaks by PXRD also confirms that the ceramic was fired below 840°C, as they would not have been detected had the ceramic been fired above 850°C (Grim and Kulbicki, 1961; Lee et al., 2008; Pérez-Monserrat et al., 2021; Trindade et al., 2009). High-temperature phases with spinel-type structure, mullite, cordierite, cristobalite, etc., were not proven in the samples (Brown and Gallagher, 2003; El Ouahabi et al., 2015). Calcium high-temperature phases such as gehlenite are also absent (Shoval and Paz, 2015). All of these phases are formed after the structural decomposition of the minerals that make up the source clay. This proves that the established calcite is not a product of the re-carbonization of degraded calcite, but is part of the source clay used to produce the ceramic (Tarhan et al., 2022) and allows for the calcite to be used to determine the firing temperature of the ceramic. Calcite was proven in all studied samples, indicating a firing temperature no higher than the calcite decomposition temperature (Table 2). The FTIR bands of illite/montmorillonite were used in order to specify the firing temperature of the samples, namely the Si-O-Si stretching vibration in the 1000-1100 cm^{-1} range and Si-O-Al bending vibration in the 510-580 cm^{-1} range. Heating to 500°C leads to the appearance of a band at 520 cm^{-1} in FTIR's spectrum. When heating above 500°C, this band disappears until reaching of 700°C when a new band appears at 570 cm^{-1} (Yan et al., 2021). In the 1000-1100 cm^{-1} spectral range, a band is registered at 1300 cm^{-1} when heating to 400°C. Heating above 500°C leads to the band shifting to higher wavenumber (Yan et al., 2021). Samples No. 92, 125, 10, 19, 29, 69, and 132 have bands between 1030-1038 cm^{-1} and 521-527 cm^{-1}, which defines their equivalent firing temperature as below 500°C. Samples No. 51 and 86 have bands between 1042-1050 cm^{-1} and no bands at 520 cm^{-1}, meaning that their equivalent firing temperature is between 500-700°C. Samples No. 38 and No.115 have a band at 1054 cm^{-1} and 570 cm^{-1}, which defines the equivalent firing temperature to be

above 700°C. The upper firing limit of these two samples is determined by the decomposition temperatures of calcite – 810.5°C and 813.2°C, respectively (Fig. 5, Table 2).

The determined equivalent firing temperatures of the ceramic also correspond to the measured LOI (Table 3). High LOI values are found to be associated with either high content of carbonate phases in the ceramic or low firing temperature of the ceramic (Daghmehchi et al., 2018). Since the carbonate content of the samples is below one percent, the high LOI values can be associated with a lower firing temperature. All samples with a specified equivalent firing temperature up to 500°C have LOI values between 8.92 and 10.26 wt%. For samples fired at a higher temperature, LOI ranged from 3.02% to 6.25 wt%. The differences in LOI values are related to the different ratio of clay/non-clay minerals in the samples. The different equivalent firing temperatures of the ceramic found in both archaeological periods suggest that the pithoi were made on-site by itinerant pithoi makers who had different skills. If prepared in a factory (specialized workshop) the pithoi would have been fired under the same conditions.

The temperatures at which the pithoi were fired confirm the lack of amorphous phases in the samples (Emami et al., 2016), which defines the ceramic as resistant over time (i.e. resistant to weathering) (Badica et al., 2022) and explains the lack of elevated background noise in the PXRD patterns (Fig. 3) (Cultrone et al., 2001; Elert et al., 2003).

4.3. Type and mineral composition of the source clay

The results of the experimental studies, together with the phase composition and equivalent firing temperatures determined by them, allowed the determination of the type of raw clay and its mineral composition.

The CaO and calcite contents of the samples indicate that the source clay used to prepare the pithoi was non-calcareous type (with CaO content less than 5% (El Ouahabi et al., 2015) or less than 6% (Maniatis and Tite, 1981). Most of the CaO is incorporated into montmorillonite, while and the calcite content is minimal at less than one percent.

The measured equivalent firing temperatures proved that no melting processes and formation of high-temperature structural synthetic phases occurred in the ceramic. In regard to this, it can be assumed that the mineral composition of the pithoi corresponds to the mineral composition of the source clay from which they are made. The only exceptions are the iron oxides, for which it cannot be determined what mineral(s) were present in the source clay. Based on this, the mineral composition of the clay can be defined as predominantly montmorillonite-illite with inclusions of non-clay minerals - quartz, feldspar, and iron oxides (hematite and/or goethite and/or magnetite).

The organic phases recorded by FTIR and thermal analysis were determined to be of secondary origin, as all the pithoi were fired at temperatures above 500°C (the decomposition of the organics takes place in the temperature range 220-420°C (Palanivel and Kumar, 2011).

4.4. Ceramic porosity

Vessels made of montmorillonite clay are durable for cooking directly over fire, while those made of kaolinite clay are impermeable as kaolinite does not shrink and swell when wet or dried (Shoval and Paz, 2015). According to the current archaeological interpretation of the settlement patterns in the studied area, agriculture was highly developed in the Roman Age, while in Late Antiquity it relied entirely on grain supplies, indicating that in both periods pithoi were vessels of considerable importance. The present studies have shown that in both periods they were made of montmorillonite-illite clay, indicating that the study of their water permeability is essential. Two main methods are implemented for testing the water absorption of modern ceramic – boiling and vacuum methods, both of which are in compliance with European standards (Wiśniewska et al., 2021). These methods measure the maximum amount of unbound water that can be physically absorbed into the pore spaces of the ceramic. The presence of pores in the ceramic controls the density of its structure and consequently its permeability (Karaman et al., 2006). When the firing temperature increases, the ceramic's porosity and ability to absorb water are reduced (Wiśniewska et al., 2021; Karaman et al., 2006). By thermal analysis, the physically absorbed water in the pores of the studied ceramics was determined, which was measured as $ML_{RT\text{-}100°C}$ (Table 2). A linear functional dependence between the amount of this water and the firing temperature of the examined pithoi sherds was found with the best fit: $y = -0.8789x + 83.387$ ($R^2 = 0.95$) (Fig. 6).

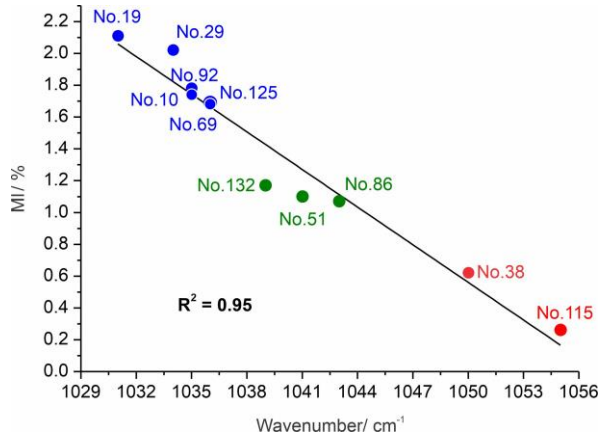

Figure 6. Wavenumber band position dependence of the $ML_{RT-100°C}$ and best fit to this data. (band position for individual samples: 1031 cm^{-1} – No. 19; 1034 cm^{-1} – No. 29; 1035 cm^{-1} – No. 10 and No. 92; 1036 cm^{-1} –No. 69 and No. 125; 1039 cm^{-1} – No. 132; 1041 cm^{-1} –No. 51; 1043 cm^{-1} – No. 86; 1050 cm^{-1} – No. 38; and 1055 cm^{-1} – No. 115). Blue – ceramic, fired at temperature under 500°C, green – firing from 500 to 700°C; red – firing between 700°C and temperature of calcite decarbonation.

The firing temperature is expressed by the shift of the illite/montmorillonite FTIR bands located near 1030 cm^{-1}. The functional dependence represents the linear decrease in the ceramic's porosity with the increase in the firing temperature – i.e., a decrease in absorbed water corresponds to a decrease in pores in the structure, which defines an increase in the density of the structure.

The obtained linear relationship confirms that the examined pithoi fragments were made of the same type of raw clay with the same mineral composition. A difference in $ML_{RT-100°C}$ was observed for the pithoi, fired at similar temperatures (Table 2). This is most likely due to a different ratio of clay/non-clay (quartz, feldspar, etc.) minerals in the source clay. This ratio is of significance as it changes the shrinkage percentage during firing, thus changing the density of the structure. The shrinkage of ceramic during firing depends not only on the firing temperature (Karaman et al., 2006) but also on the percentage of non-clay minerals. The increased amount of non-clay minerals increases the number of pores in the ceramic and leads to a higher water absorption capacity (Cultrone et al., 2001). The different ratio of clay/non clay minerals may be due to natural variations in different areas of the source clay deposit (Chamley, 1989) and/or due to the use of clay from different deposits; and/or the mixing of clay from different deposits. The issue cannot be resolved unequivocally because (i) concentrations of minor (rare) elements do not provide specific information on the source material deposit: Cu, Zn, Rb, Sr, and Zr were found in all samples; Cr and Ag were identified in single samples, also in minimal amounts, and cannot be considered as significant (Table 3); the concentrations of the main elements are too close; (iii) the geological data for the studied area show that clays have been described at only one of the archaeological sites (No. 8).

5. CONCLUSIONS

The following results were obtained from the archaeometric study of the pithoi:

- The mineral composition of the pithoi was determined – quartz, feldspars, hematite, calcite, illite, montmorillonite, muscovite, with a predominant montmorillonite content from the clay minerals. Each of the minerals is registered by different methods, which justifies the need to use a complex of analytical methods for such a study. Quartz has been proven by PXRD, FTIR, and thermal analysis (registered by α-β quartz transition). Albite – by PXRD and FTIR, microcline – only by FTIR due to its small amounts in the samples. Calcite was proven by FTIR and thermal analysis. The percentage of calcite in the samples was also calculated, ranging from 0.18 to 0.92% using ML_{CO2} measured by thermal analysis. Its low content explains the lack of calcite reflections in PXRD and the low-intensity bands in FTIR. Hematite was only recorded by FTIR and thermal analysis (PXRD cannot register hematite due to the measurement conditions – CuKα radiation). The phyllosilicates were proven by PXRD, FTIR, and thermal analysis, and the XRF results support them by the measured contents of K_2O, MgO, CaO, and the Si/Al ratio (Al_2O_3/SiO_2). The predominant montmorillonite content was determined by FTIR.
- The equivalent firing temperatures of the pithoi were determined – two of the samples were fired in the temperature range up to 500°C, seven were fired at temperatures between 500 and 700°C; two were fired in the range 700°C – thermal decomposition temperature of calcite. The equivalent firing temperatures were established by the mineral composition of the pithoi determined by the full range of analytical methods, as well as by the FTIR bands of illite/montmorillonite – Si-O-Si stretching vibration in the 1000-1100 cm^{-1} range and Si-O-Al bending vibration in the 510-580 cm^{-1} range. The determined equivalent firing temperatures are confirmed by the LOI values measured by thermal analysis.
- The type and mineral composition of the source clay was determined by the results obtained for the mineral composition and equivalent firing temperature of the ceramic. The source clay was determined to be non-calcareous type according

to the CaO content included in carbonate minerals (less than 1 wt%), as determined from thermal analysis by measuring the mass loss of calcite decomposition in the temperature range 770-840°C. In comparison, the XRF data show a CaO content in the pithoi between 1.2 and 2.5 wt%, thus demonstrating the need to also use thermal analysis to determine the clay type. The mineral composition of the source clay was determined to be montmorillonite-illite with variable contents of non-clay minerals (muscovite, quartz, albite, microcline, iron oxides, calcite).

The advantages of the thermal method were used to determine LOI and estimate the density of the ceramic structure in relation to its permeability. Thermal analysis data for LOI determination has the advantage of being able to separate different processes over different temperature ranges. In addition, it can determine what temperature the samples should be heated to in order to correctly estimate LOI values. That is, for each particular material studied, it is appropriate to determine at what temperature crystallization processes associated with oxygen uptake and sample weight increase begin. The determined linear functional relationship between ML_{RT-100} and the firing temperature of the ceramic indicates the water-absorbing properties of fired illite-montmorillonite clay with different clay/non-clay minerals ratios.

The use of identical montmorillonite-illite source material with varying ratios of non-clay minerals and three different firing temperature ranges was established for all archaeological sites during both periods. The different firing temperatures suggest on-site production by itinerant craftsmen with different skills, a tradition that has persisted from the Roman Age to Late Antiquity. The use of the same type of raw material in both periods, without a specific locality for its extraction, shows continuity in people's knowledge of the environment.

The results obtained, together with the earlier results for bricks and tiles (Kostova et al., 2023b) and mortar (Kostova et al., 2023a) from the sites in the same area, support the archaeological view of a transformation of Roman economic patterns in Late Antiquity due to a financial and economic crisis without the realization of any demographic changes.

The obtained results are new for pithoi from Bulgarian archaeological sites and complement the sporadic experimental data in the literature regarding pithoi produced after the Bronze Age. In addition, they allow for conservation and restoration work to be carried out.

The results obtained from the archaeometric study of the pithoi provide a perspective for future research:

- The data obtained on the mineral composition of the source clay will enable a successful search for a raw material source over an extended geographical area. Locating the clay deposit will provide additional archaeological information as the choice of deposit in the past may have been influenced by a variety of factors – land ownership and control, seasonal access, ground surface exposure, transportability, etc. (Xanthopoulou et al., 2020; Liritzis et al., 2020a; Liritzis et al., 2020b).
- Should a raw material source be found, further research is planned so as to expand knowledge on the production technology of pithoi:
  - Study of the clay by the experimental methods used and comparison with the results obtained from the study of the ceramic. Use of additional analysis - petrographic, to study inclusions and determine their genesis.
  - More accurate determination of the equivalent firing temperatures by examining and comparing the ceramic (reheated) and clay (heated under controlled conditions) by scanning electron microscopy (SEM) (Tite, 1992; Pollard et al., 2007).
  - Study of the clay by XRF and comparison of the results with those obtained for the ceramic by using binary diagrams, and application of statistical hierarchical cluster analysis of trace elements to determine the provenance of the ceramic (Liritzis et al., 2020a; Liritzis et al., 2020b). Trace elements are essential for obtaining these results, as their geochemical behavior in a sedimentary setting (at the Earth's surface) is predictable (Pollard et al., 2007; Bauer and Velde, 2014).

Author Contributions: Conceptualization, B.K., K.M. and B.D.; methodology, B.K and K.M.; software, K.M.; validation, B.K., K.M. and B.D.; formal analysis, B.K. and K.M.; investigation, B.K. and K.M.; resources, B.D. and B.K.; data curation, R.B.; writing—original draft preparation, B. K., K.M. and B. D.; writing—review and editing, K.M.; visualization, R.B.; supervision, B.D..; project administration, B.K. and B.D.; funding acquisition, B.D. All authors have read and agreed to the published version of the manuscript.

ACKNOWLEDGEMENTS

This work was funded by the National Science Fund of Bulgaria under grant KP-06-N80/5 (B.K., B.D). The authors gratefully acknowledge New Bulgarian University, the Department of Natural Sciences and the Geology laboratory – BF.

REFERENCES

Altomare, A., Cuocci, C., Giacovazzo, C., Moliterni, A. and Rizzi, R. (2008) QUALX: a computer program for qualitative analysis using powder diffraction data. *Journal of Applied Crystallography*, Vol. 41, No. 4, 815–817. https://doi.org/10.1107/s0021889808016956

Annamalai, G. R., Ravisankar, R., Naseerutheen, A., Chandrasekaran, A. and Rajan, K. (2014) Application of various spectroscopic techniques to characterize the archaeological pottery excavated from Manaveli, Puducherry, India. *Optik*, Vol. 125, No. 21, 6375–6378. https://doi.org/10.1016/j.ijleo.2014.06.099

Aras, A. and Kiliç, S. (2017) The mineralogy and firing behaviour of pottery clays of the Lake Van region, eastern Turkey. *Clay Minerals*, Vol. 52, No. 4, 453–468. https://doi.org/10.1180/claymin.2017.052.4.04

Badica, P., Alexandru-Dinu, A., Grigoroscuta, M. A., Burdusel, M., Aldica, G. V., Sandu, V., Bartha, C., Polosan, S., Galatanu, A., Kuncser, V., Enculescu, M., Locovei, C., Porosnicu, I., Tiseanu, I., Ferbinteanu, M., Savulescu, I., Negru, M. and Batalu, N. D. (2022) Mud and burnt Roman bricks from Romula. *Scientific Reports*, Vol. 12, No. 1. https://doi.org/10.1038/s41598-022-19427-7

Bauer, A. and Velde, B. D. (2014) *Geochemistry at the Earth's surface: Movement of Chemical Elements* Berlin, Heidelberg, Springer.

Bergaya, F., Theng, B. K. G. and Lagaly, G. (2006) *Handbook of Clay Science,* Amsterdam, Elsevier Science.

Bevan, A. (2017) Pandora's pithos. *History and Anthropology*, Vol. 29, No. 1, 7–14. https://doi.org/10.1080/02757206.2017.1397651

Bitay, E., Kacsó, I., Tănăselia, C., Toloman, D., Borodi, G., Pánczél, S., Kisfaludi-Bak, Z. and Veress, E. (2020) Spectroscopic Characterization of Iron Slags from the Archaeological Sites of Brâncoveneşti, Călugăreni and Vătava Located on the Mureş County (Romania) Sector of the Roman Limes. *Applied Sciences*, Vol. 10, No. 15, 5373. https://doi.org/10.3390/app10155373

Böke, H., Akkurt, S., İpekoğlu, B. and Uğurlu, E. (2006) Characteristics of brick used as aggregate in historic brick-lime mortars and plasters. *Cement and Concrete Research*, Vol. 36, No. 6, 1115–1122. https://doi.org/10.1016/j.cemconres.2006.03.011

Boyanov, I. (2014) *Diskoduratere and the Emporia in Roman Thrace* Sofia, Avalon Publishing.

Boyanov, I., Goranov, A., Shilyafova, Z. and Ruseva, M. (1991) *Map Sheet Dimitrovgrad*.

Boyanov, I., Shilyafova, Z., Goranov, A., Ruseva, M. and Nenov, T. (1993) *Map Sheet Chirpan*.

Bradley, W. F. and Grim, R. E. (1951) High temperature thermal effects of clay and related materials. *American Mineralogist*, Vol. 36, No. 3-4, 182–201.

Brown, M. E. and Gallagher, P. K. (2003) *Handbook of Thermal Analysis and Calorimetry: Applications to inorganic and miscellaneous materials* Amsterdam, Elsevier Science.

Caccamo, M. T., Mavilia, G., Mavilia, L., Lombardo, D. and Magazù, S. (2020) Self-Assembly processes in hydrated montmorillonite by FTIR investigations. *Materials*, Vol. 13, No. 5, 1100. https://doi.org/10.3390/ma13051100

Cardiano, P., Ioppolo, S., De Stefano, C., Pettignano, A., Sergi, S. and Piraino, P. (2004) Study and characterization of the ancient bricks of monastery of "San Filippo di Fragalà" in Frazzanò (Sicily). *Analytica Chimica Acta*, Vol. 519, No. 1, 103–111. https://doi.org/10.1016/j.aca.2004.05.042

Chamley, H. (1989) *Clay Sedimentology* Berlin, Heidelberg, Springer.

Chukanov, N. V. (2014) *Infrared spectra of mineral species: Extended library* Berlin, Heidelberg, Springer.

Chukanov, N. V. and Chervonnyi, A. D. (2016) *Infrared spectroscopy of minerals and related compounds* Springer.

Cultrone, G., Rodriguez-Navarro, C., Sebastian, E., Cazalla, O. and De La Torre, M. J. (2001) Carbonate and silicate phase reactions during ceramic firing. *European Journal of Mineralogy*, Vol. 13, No. 3, 621–634. https://doi.org/10.1127/0935-1221/2001/0013-0621

Daghmehchi, M., Rathossi, C., Omrani, H., Emami, M. and Rahbar, M. (2018) Mineralogical and thermal analyses of the Hellenistic ceramics from Laodicea Temple, Iran. *Applied Clay Science*, Vol. 162, 146–154. https://doi.org/10.1016/j.clay.2018.06.007

Derkowski, A. and Kuligiewicz, A. (2022) Thermal Analysis and Thermal Reactions of Smectites: a Review of Methodology, Mechanisms, and Kinetics. *Clays and Clay Minerals*, Vol. 70, No. 6, 946–972. https://doi.org/10.1007/s42860-023-00222-y

Drebushchak, V. A., Mylnikova, L. N., Drebushchak, T. N. and Boldyrev, V. V. (2005) The investigation of ancient pottery. *Journal of Thermal Analysis and Calorimetry*, Vol. 82, No. 3, 617–626. https://doi.org/10.1007/s10973-005-0942-9

Dumanov, B. (2005) Rescue Archaeological Excavations of Site N 13A near the Village of Malko Tranovo, Chirpan Municipality. *Archaeological Discoveries and Excavation*, 243–244.

Dumanov, B. (2017) *The Settlement Complex near the Village of Gorno Novo Selo-a Regional Administrative, Economic and Religious Center in the Central Part of Sarnena Sredna Gora. SARCHUS-AIR. Localization and experimental reconstruction of ancient roads and habitats* Askoni-Izdat.

El Ouahabi, M. E., Daoudi, L., Hatert, F. and Fagel, N. (2015) Modified mineral phases during clay ceramic firing. *Clays and Clay Minerals*, Vol. 63, No. 5, 404–413. https://doi.org/10.1346/ccmn.2015.0630506

Elert, K., Cultrone, G., Navarro, C. R. and Pardo, E. S. (2003) Durability of bricks used in the conservation of historic buildings — influence of composition and microstructure. *Journal of Cultural Heritage*, Vol. 4, No. 2, 91–99. https://doi.org/10.1016/s1296-2074(03)00020-7

Emami, M., Sakali, Y., Pritzel, C. and Trettin, R. (2016) Deep inside the ceramic texture: A microscopic–chemical approach to the phase transition via partial-sintering processes in ancient ceramic matrices. *Journal of Microscopy and Ultrastructure*, Vol. 4, No. 1, 11. https://doi.org/10.1016/j.jmau.2015.08.003

Fierascu, R. C., Fierascu, I., Baroi, A. M., Brazdis, R. I., Fistos, T., Nicolae, C. A., Raditoiu, V., Inel, I. C. and Sava, V. (2020) Characterization of historical ceramics: a case study. *Romanian Reports in Physics*, 801.

File, P. D. (2001) *International Centre for Diffraction Data (ICDD) Newtown Square* [Software]. Powder Diffraction File (PDF): Newtown Square, PA, USA.

Földvári, M. (2011) *Handbook of Thermogravimetric System of Minerals and its Use in Geological Practice* Budapest, Geological Institute of Hungary.

Frangipane, G., Pistolato, M., Molinaroli, E., Guerzoni, S. and Tagliapietra, D. (2008) Comparison of loss on ignition and thermal analysis stepwise methods for determination of sedimentary organic matter. *Aquatic Conservation*, Vol. 19, No. 1, 24–33. https://doi.org/10.1002/aqc.970

Garg, N. and Skibsted, J. (2015) Heated Montmorillonite: structure, reactivity, and dissolution. In *Rilem bookseries*, 117–124. https://doi.org/10.1007/978-94-017-9939-3_15

Garrison, E. (2016) *Techniques in Archaeological Geology* Springer.

Giannopoulou, M. (2010) *Pithoi: Technology and History of Storage Vessels Through the Ages* British Archaeological Reports Limited.

Grim, R. E. and Kulbicki, G. (1961) Montmorillonite: high temperature reactions and classification. *American Mineralogist*, Vol. 46, 1329–1369. https://pubs.geoscienceworld.org/msa/ammin/article-abstract/46/11-12/1329/541844/Montmorillonite-high-temperature-reactions-and

Hamilton, A. and Hall, C. (2012) A review of rehydroxylation in Fired-Clay ceramics. *Journal of the American Ceramic Society*, Vol. 95, No. 9, 2673–2678. https://doi.org/10.1111/j.1551-2916.2012.05298.x

Hatakeyama, T. and Liu, Z. (1998) *Handbook of Thermal Analysis* Chichester, Wiley.

Ion, R., Ion, M., Fierascu, R. C., Serban, S., Dumitriu, I., Radovici, C., Bauman, I., Cosulet, S. and Niculescu, V. I. R. (2010) Thermal analysis of Romanian ancient ceramics. *Journal of Thermal Analysis and Calorimetry*, Vol. 102, No. 1, 393–398. https://doi.org/10.1007/s10973-009-0226-x

Jozanikohan, G. and Abarghooei, M. N. (2022) The Fourier transform infrared spectroscopy (FTIR) analysis for the clay mineralogy studies in a clastic reservoir. *Journal of Petroleum Exploration and Production Technology*, Vol. 12, No. 8, 2093–2106. https://doi.org/10.1007/s13202-021-01449-y

Karaman, S., Ersahin, S. and Gunal, H. (2006) Firing temperature and firing time influence on mechanical and physical properties of clay bricks. *Journal of Scientific and Industrial Research*, Vol. 65, No. 2, 153–159.

Kenkel, J. (2013) *Analytical Chemistry for Technicians, Fourth Edition* CRC Press.

Khalifa, A. Z., Pontikes, Y., Elsen, J. and Cizer, Ö. (2019) Comparing the reactivity of different natural clays under thermal and alkali activation. *RILEM Technical Letters*, Vol. 4, 74–80. https://doi.org/10.21809/rilemtechlett.2019.85

Kibaroğlu, M. and Thumm-Doğrayan, D. (2013) Trojan pithoi: A petrographic approach to provenance of Bronze Age storage vessels from Troy. *Applied Clay Science*, Vol. 82, 44–52. https://doi.org/10.1016/j.clay.2013.06.023

King, B. and Vivit, D. (1988) Loss-on-ignition corrections in the XRF analysis of silicate rocks. *X-ray Spectrometry/X-Ray Spectrometry*, Vol. 17, No. 4, 145–147. https://doi.org/10.1002/xrs.1300170406

Kloužková, A., Kavanová, M., Kohoutková, M., Zemenová, P. and Dragoun, Z. (2016) Identification of causes of degradation of Gothic ceramic tiles by thermal analyses. *Journal of Thermal Analysis and Calorimetry*, Vol. 125, No. 3, 1311–1318. https://doi.org/10.1007/s10973-016-5488-5

Kostova, B., Dumanov, B. and Mihaylova, K. (2023) Archaeological Bricks and Tiles from Southeast Bulgaria-Determination of Raw Material and Production Technology by Chemical, Phase, and Thermal Analyses. *Mediterranean Archaeology and Archaeometry*, Vol. 23, No. 2, 1-22. https://doi.org/10.5281/zenodo.7870973

Kostova, B., Dumanov, B., Stoyanov, V. and Shivachev, B. (2022) Thermal and phase analysis of Roman and Late Antiquity mortars from Bulgarian archaeological sites. *Journal of Thermal Analysis and Calorimetry*, Vol. 148, No. 4, 1543–1555. https://doi.org/10.1007/s10973-022-11493-3

Kotryová, B., Ondruška, J., Štubňa, I. and Bačík, P. (2016) Thermoanalytical investigation of ancient pottery. *AIP Conference Proceedings*. https://doi.org/10.1063/1.4955247

Labus, M., Matyasik, I. and Ziemianin, K. (2023) Thermal decomposition processes in relation to the type of organic matter, mineral and maceral composition of menilite shales. *Energies*, Vol. 16, No. 11, 4500. https://doi.org/10.3390/en16114500

Lee, W., Souza, G., McConville, C., Tarvornpanich, T. and Iqbal, Y. (2008) Mullite formation in clays and clay-derived vitreous ceramics. *Journal of the European Ceramic Society*, Vol. 28, No. 2, 465–471. https://doi.org/10.1016/j.jeurceramsoc.2007.03.009

Liritzis, I., Xanthopoulou, V., Palamara, E., Papageorgiou, I., Iliopoulos, I., Zacharias, N., Vafiadou, A. and Karydas, A. G. (2020a) Characterization and provenance of ceramic artifacts and local clays from Late Mycenaean Kastrouli (Greece) by means of p-XRF screening and statistical analysis. *Journal of Cultural Heritage*, Vol. 46, 61–81. https://doi.org/10.1016/j.culher.2020.06.004

Liritzis, I., Laskaris, N., Vafiadou, A., Karapanagiotis, I., Volonakis, P., Papageorgopoulou, C. and Bratitsi, M. (2020b) Archaeometry: an overview. *Scientific culture*, Vol. 6, No. 1, 49-98. DOI: 10.5281/zenodo.3625220

Lis, B. and Rückl, Š. (2011) Our Storerooms Are Full. Impressed Pithoi from Late Bronze/Early Iron Age East Lokris and Phokis and Their Socio-economic Significance. In: *Our Cups Are Full: Pottery and Society in the Aegean Bronze Age. Papers Presented to Jeremy B. Rutter on the Occasion of His 65th Birthday*, W. Gauss, M. Lindblom, R.A.K. Smith, and J. C. Wright (eds.), BAR International Series 2227, Oxford, 154–168.

Liu, D., Yuan, P., Liu, H., Cai, J., Qin, Z., Tan, D., Zhou, Q., He, H. and Zhu, J. (2011) Influence of heating on the solid acidity of montmorillonite: A combined study by DRIFT and Hammett indicators. *Applied Clay Science*, Vol. 52, No. 4, 358–363. https://doi.org/10.1016/j.clay.2011.03.016

Liu, H., Chen, T., Zou, X., Qing, C. and Frost, R. L. (2013) Thermal treatment of natural goethite: Thermal transformation and physical properties. *Thermochimica Acta*, Vol. 568, 115–121. https://doi.org/10.1016/j.tca.2013.06.027

Maniatis, Y. and Tite. (1981) Technological examination of Neolithic-Bronze Age pottery from central and southeast Europe and from the Near East. *Journal of Archaeological Science*, Vol. 8, No. 1, 59–76. https://doi.org/10.1016/0305-4403(81)90012-1

Marsh, A., Heath, A., Patureau, P., Evernden, M. and Walker, P. (2018) Alkali activation behaviour of un-calcined montmorillonite and illite clay minerals. *Applied Clay Science*, Vol. 166, 250–261. https://doi.org/10.1016/j.clay.2018.09.011

McLoughlin, B. (2015) *Searching for the potter's intention: the pithos makers of Zagora* University of Sydney.

Meunier, A. and Albani, A. E. (2007) The glauconite–Fe-illite–Fe-smectite problem: a critical review. *Terra Nova*, Vol. 19, No. 2, 95–104. https://doi.org/10.1111/j.1365-3121.2006.00719.x

Moropoulou, A., Bakolas, A. and Bisbikou, K. (1995) Characterization of ancient, byzantine and later historic mortars by thermal and X-ray diffraction techniques. *Thermochimica Acta*, Vol. 269–270, 779–795. https://doi.org/10.1016/0040-6031(95)02571-5

Muller, F., Plançon, A. and Robert, J.-L. (2000) Structural Transformation of 2:1 Dioctahedral Layer Silicates during Dehydroxylation-Rehydroxylation Reactions. *Clays and Clay Minerals*, Vol. 48, No. 5, 572–585. https://doi.org/10.1346/ccmn.2000.0480510

Nagwa, S. and Abdel Rahim (2016) Analytical study and conservation of archaeological terra sigıllata ware from roman period, tripoli, Libya. *Scientific culture*, Vol. 2, No 2, 19-27. DOI: 10.5281/zenodo.44896

Nikolov, D. (1984) Trakyiskata vila pri Chatalka, Starozagorsko (Thracian villa at Chatalka, Stara Zagora). *Discoveries and Excavation*, Vol. 7.

Palanivel, R. and Kumar, R. (2011) Thermal and spectroscopic analysis of ancient potteries. *Romanian Journal of Physics*, Vol. 56, No. 1-2, 195–208.

Papadopoulou, D. N., Lalia-Kantouri, M., Kantiranis, N. and Stratis, J. A. (2006) Thermal and mineralogical contribution to the ancient ceramics and natural clays characterization. *Journal of Thermal Analysis and Calorimetry*, Vol. 84, No. 1, 39–45. https://doi.org/10.1007/s10973-005-7173-y

Pei, Z., Lin, M., Liu, Y. and Lei, S. (2018) Dissolution Behaviors of Trace Muscovite during Pressure Leaching of Hydrothermal Vein Quartz Using H_2SO_4 and NH_4Cl as Leaching Agents. *Minerals*, Vol. 8, No. 2, 60. https://doi.org/10.3390/min8020060

Pérez-Monserrat, E. M., Maritan, L., Garbin, E. and Cultrone, G. (2021) Production Technologies of Ancient Bricks from Padua, Italy: Changing Colors and Resistance over Time. *Minerals*, Vol. 11, No. 7, 744. https://doi.org/10.3390/min11070744

Pollard, A. M., Batt, C. M., Stern, B. and Young, C. M. M. (2007) *Analytical chemistry in Archaeology, First edition* Cambridge University Press.

Ponomar, V. (2018) Thermomagnetic properties of the goethite transformation during high-temperature treatment. *Minerals Engineering*, Vol. 127, 143–152. https://doi.org/10.1016/j.mineng.2018.08.016

Porta, F. (2021) The Use of the Wheel in the Production of Pithoi: Preliminary Results and Lessons Learnt from Experimental Sessions. *Interdisciplinaria Archaeologica*, Vol. 12, No. 2, 155–171. https://doi.org/10.24916/iansa.2021.2.4

Ramos, S. S., Reig, F. B., Adelantado, J. G., Marco, D. Y. and Carbó, A. D. (2002) Application of XRF, XRD, thermal analysis, and voltammetric techniques to the study of ancient ceramics. *Analytical and Bioanalytical Chemistry*, Vol. 373, No. 8, 893–900. https://doi.org/10.1007/s00216-002-1376-x

Rao, H., Yang, Y., Hu, X., Yu, J. and Jiang, H. (2017) Identification of an Ancient Birch Bark Quiver from a Tang Dynasty (A.D. 618–907) Tomb in Xinjiang, Northwest China. *Economic Botany*, Vol. 71, No. 1, 32–44. https://doi.org/10.1007/s12231-017-9369-z

Ravisankar, R., Kiruba, S., Eswaran, P., Senthilkumar, G. and Chandrasekaran, A. (2010) Mineralogical Characterization studies of Ancient potteries of Tamilnadu, India by FT-IR Spectroscopic Technique. *E-Journal of Chemistry*, Vol. 7, No. 1, 185–190. https://doi.org/10.1155/2010/643218

Shaltout, A. A., Gomma, M. M. and Ali-Bik, M. W. (2012) Utilization of standardless analysis algorithms using WDXRF and XRD for Egyptian iron ore identification. *X-Ray Spectrometry*, Vol. 41, No. 6, 355–362. https://doi.org/10.1002/xrs.2410

Shoval, S. and Paz, Y. (2015) Analyzing the fired-clay ceramic of EBA Canaanite pottery using FT-IR spectroscopy and LA-ICP-MS. *Periodico Di Mineralogia*, Vol. 84, No. 1. https://doi.org/10.2451/2015pm0011

Sugawara, T. (2000) Thermodynamic analysis of Fe and Mg partitioning between plagioclase and silicate liquid. *Contributions to Mineralogy and Petrology*, Vol. 138, No. 2, 101–113. https://doi.org/10.1007/s004100050011

Tarhan, İ., Massa, M., Tuna, Y. and Şahin, F. (2022) An archaeometric study of the Konya basin metallic ware through FTIR and XRD analysis with chemometrics: Central Anatolian Early Bronze Age ceramics. *Archaeometry*, Vol. 65, No. 1, 136–150. https://doi.org/10.1111/arcm.12812

Tite, M. S. (1992) The Impact of Electron Microscopy on Ceramic Studies. *Proceedings of the British Academy*, Vol. 77, 111–131.

Trindade, M., Dias, M., Coroado, J. and Rocha, F. (2009) Mineralogical transformations of calcareous rich clays with firing: A comparative study between calcite and dolomite rich clays from Algarve, Portugal. *Applied Clay Science*, Vol. 42, No. 3-4, 345–355. https://doi.org/10.1016/j.clay.2008.02.008

Tsankov, T., Filipov, L. and Katskov, N. (1995) *Map Sheet Stara Zagora*.

Waiman-Barak, P., Susnow, M., Nickelsberg, R., Cline, E. H., Yasur-Landau, A. and Shahack-Gross, R. (2018) Technological aspects of Middle Bronze Age II production of pithoi at Tel Kabri, Israel: specialized pottery production in a palatial system. *Levant*, Vol. 50, No. 1, 32–51. https://doi.org/10.1080/00758914.2018.1545509

Wendel, M. (2020) *Die Rettungsgrabungen auf der Autobahntrasse "Trakija" bei Karasura 1987-1990 (ZAKS-Schriften 23): Karasura IV*.

Wiśniewska, K., Pichór, W. and Kłosek-Wawrzyn, E. (2021) Influence of firing temperature on phase composition and color properties of ceramic tile bodies. *Materials*, Vol. 14, No. 21, 6380. https://doi.org/10.3390/ma14216380

Xanthopoulou, V., Iliopoulos, I., Katsonopoulou, D. and Katsarou, S. (2022) Standardized patterns in the ceramic craft at Early Bronze Age Helike, Achaea, Greece. *Archaeological and Anthropological Sciences*, Vol. 14, No. 8. https://doi.org/10.1007/s12520-022-01621-3

Xanthopoulou, V., Iliopoulos, I. and Liritzis, I. (2020) Characterization Techniques of Clays for the Archaeometric Study of Ancient Ceramics: a Review. *Scientific Culture*, Vol. 6, No. 2, 73–86. https://doi.org/10.5281/ZENODO.3724849

Ximeri, S. (2017) Pithos (storage vessel). *The Encyclopedia of Ancient History*, Vol. 1. https://doi.org/10.1002/9781444338386.wbeah30456

Yan, B., Liu, S., Chastain, M. L., Yang, S. and Chen, J. (2021) A new FTIR method for estimating the firing temperature of ceramic bronze-casting moulds from early China. *Scientific Reports*, Vol. 11, No. 1. https://doi.org/10.1038/s41598-021-82806-z